

## Supporting information

# Constructing Vertically Aligned ZIF-67 Microrod Arrays on Carbon Cloth with Commercial-level Mass-loading for High-performance Supercapacitors

Chenchen Bai,<sup>a</sup> Bingjun Li,<sup>a</sup> Dejun Li,<sup>a</sup> Yan Han <sup>\*a</sup> and Caiyun Wang <sup>\*b</sup>

<sup>a</sup> College of Physics and Materials Science, Tianjin Normal University, Tianjin 300387, China

<sup>b</sup> Faculty of Engineering and Information Sciences, University of Wollongong, New South Wales  
2500, Australia

**Fig. S1** (a, b) SEM images and (c, d) capacitive performances of Co/CC immersed in a 2-MeIM aqueous solution for 24 h followed by adding  $\text{Co}(\text{NO}_3)_2 \cdot 6\text{H}_2\text{O}$  aqueous solution for another 24 h (a, c) and 72 h (b, d).

**Fig. S2** (a-d) SEM images of bare CC (a, b) and Co/CC (c, d). (e) EDS mappings of Co/CC.

**Fig. S3** XRD pattern of Co/CC.

**Fig. S4** (a) SEM image and (b) EDS mappings of ZIF-67/CC-24.

**Fig. S5** TEM image of ZIF-67/CC.

**Fig. S6** Digital photographs of ZIF-67 grown on bare CC and Co-covered CC: (a) bare CC immersed in an aqueous solution containing 2-MeIM and  $\text{Co}(\text{NO}_3)_2 \cdot 6\text{H}_2\text{O}$  for 72 h; (b) Co/CC immersed in a 2-MeIM aqueous solution for 72 h; (c) Co/CC immersed in a 2-MeIM aqueous solution for 24 h followed by adding  $\text{Co}(\text{NO}_3)_2 \cdot 6\text{H}_2\text{O}$  aqueous solution for another 48 h.

**Fig. S7** (a) SEM image and (b) EDS mappings of ZIF-67/CC-NC.

**Fig. S8** Full scan survey XPS spectrum for ZIF-67/CC-24.

**Fig. S9** High-resolution XPS C1s spectrum of ZIF-67/CC.

**Fig. S10** TGA curves of ZIF-67/CC, CC and ZIF-67 powders.

**Fig. S11** (a) XPS spectra of Co 2p and (b) XRD pattern of ZIF-67/CC electrode after cycling.

**Fig. S12** (a) CV curves of AC/CC electrode at different scan rates. (b) Galvanostatic charge-discharge curves of AC/CC electrode at different current densities.

**Fig. S13** CV curves of ZIF-67/CC//AC/CC ASSC device collected within different potential windows at  $10 \text{ mV s}^{-1}$ .

**Fig. S14** Cycling performance of ZIF-67/CC//AC/CC ASSC device at  $10 \text{ mA cm}^{-2}$ .

**Fig. S15** Nyquist plot of the ASSC device.

**Table S1** Capacitive performance comparison of reported MOF materials.

**Table S2** Comparison of areal energy and power densities for some reported MOF-based devices.

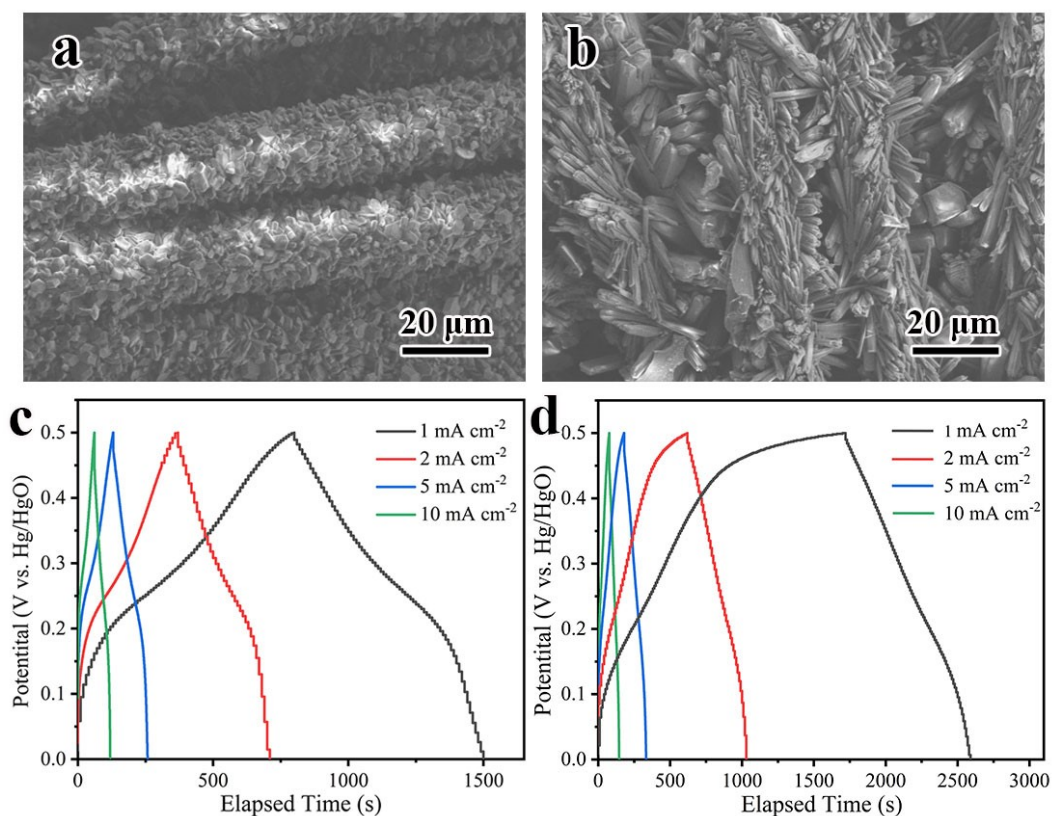


**Fig. S1** (a, b) SEM images and (c, d) capacitive performances of Co/CC immersed in a 2-MeIM aqueous solution for 24 h followed by adding  $\text{Co}(\text{NO}_3)_2 \cdot 6\text{H}_2\text{O}$  aqueous solution for another 24 h (a, c) and 72 h (b, d).

The immersion time of Co/CC was optimized to regulate the ZIF-67 mass-loading on CC in preliminary experiments. It was observed from SEM images that the morphology of samples obtained at different immersion time was different. A shorter immersion time (ZIF-67/CC-24, Fig. S1a) was not helpful to preferred orientation growth of ZIF-67, whereas a longer time (ZIF-67/CC-72, Fig. S1b) caused the bundled formation of ZIF-67 rods. The ZIF-67 mass-loading of ZIF-67/CC-24 and ZIF-67/CC-72 was about 6 and 20  $\text{mg cm}^{-2}$ , respectively. The areal specific capacitances of ZIF-67/CC-24 were about 1400, 1360, 1270 and 1180  $\text{mF cm}^{-2}$  at 1, 2, 5 and 10  $\text{mA cm}^{-2}$ . The corresponding gravimetric specific capacitances were 233, 227, 212 and 197  $\text{F g}^{-1}$ , respectively. For ZIF-67/CC-72 with higher mass-loading, the areal specific capacitances were 1740, 1640, 1530 and 1380  $\text{mF cm}^{-2}$  at 1, 2, 5 and 10  $\text{mA cm}^{-2}$ .

While the gravimetric specific capacitances dropped to 87, 82, 77 and 69 F g<sup>-1</sup>, respectively. Therefore, the change of capacitive performances was not only due to the variation of mass-loading but also the different morphology.

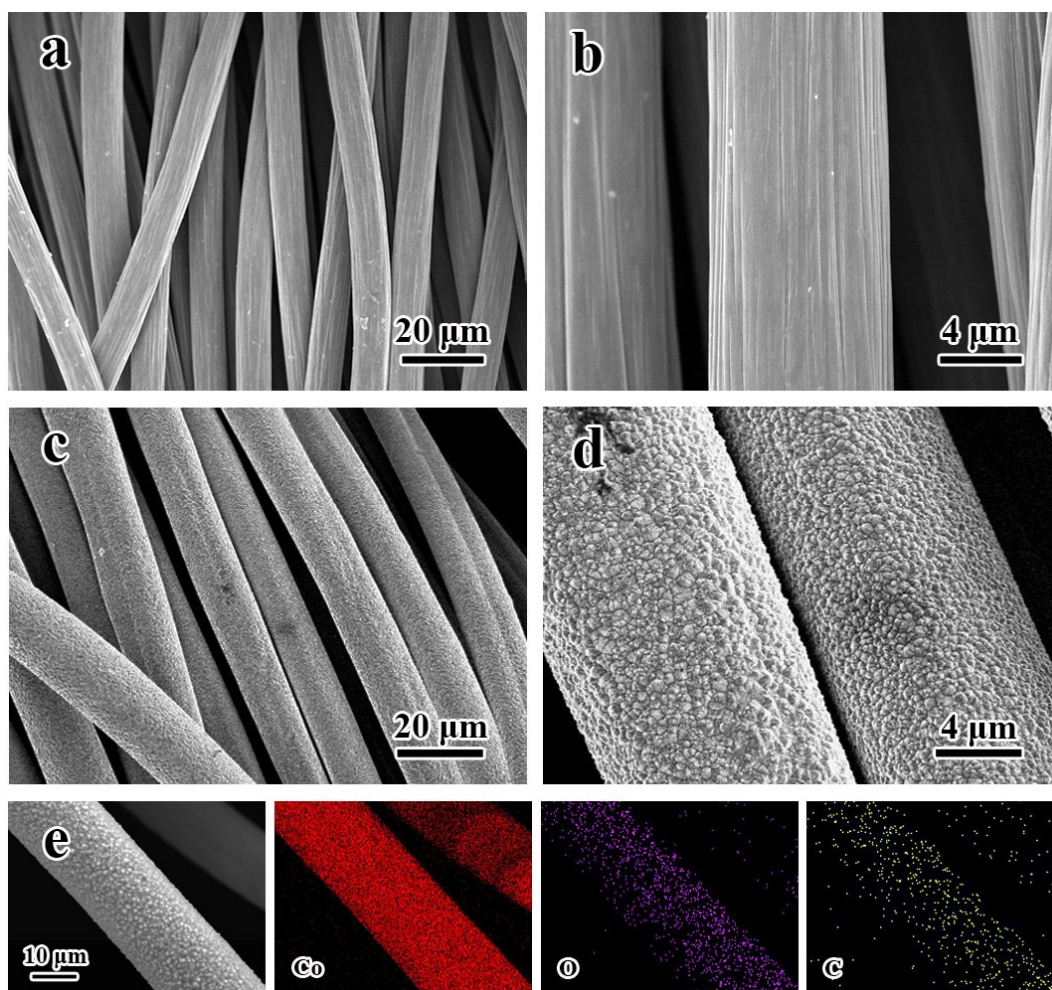


**Fig. S2** (a-d) SEM images of bare CC (a, b) and Co/CC (c, d). (e) EDS mappings of Co/CC.

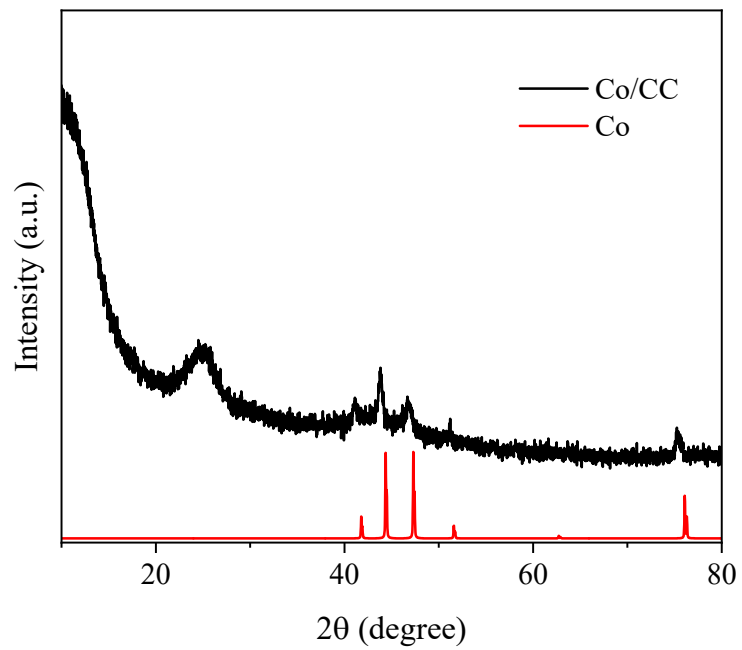


**Fig. S3** XRD pattern of Co/CC.

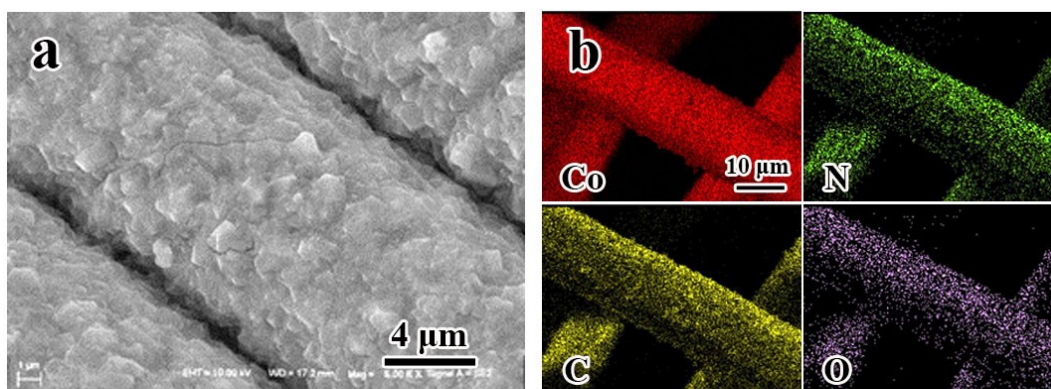


**Fig. S4** (a) SEM image and (b) EDS mappings of ZIF-67/CC-24.

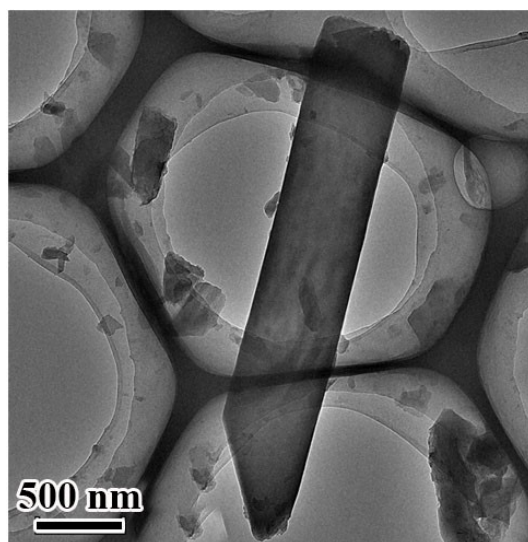


**Fig. S5** TEM image of ZIF-67/CC.

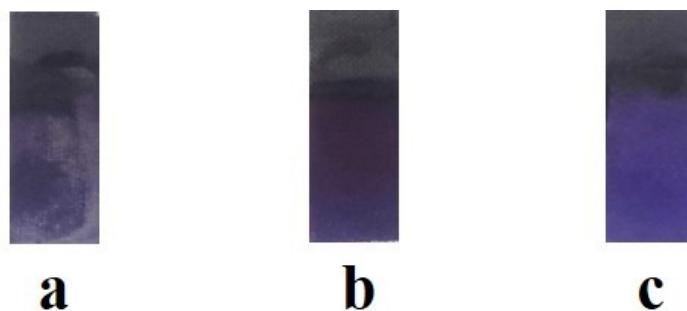


**Fig. S6** Digital photographs of ZIF-67 grown on bare CC and Co-covered CC: (a) bare CC immersed in an aqueous solution containing 2-MeIM and  $\text{Co}(\text{NO}_3)_2 \cdot 6\text{H}_2\text{O}$  for 72 h; (b) Co/CC immersed in a 2-MeIM aqueous solution for 72 h; (c) Co/CC immersed in a 2-MeIM aqueous solution for 24 h followed by adding  $\text{Co}(\text{NO}_3)_2 \cdot 6\text{H}_2\text{O}$  aqueous solution for another 48 h.



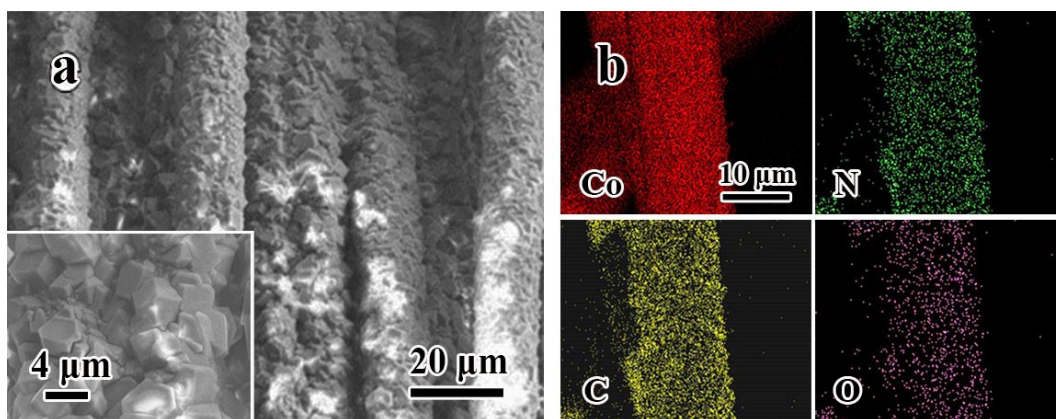


**Fig. S7** (a) SEM image and (b) EDS mappings of ZIF-67/CC-NC.

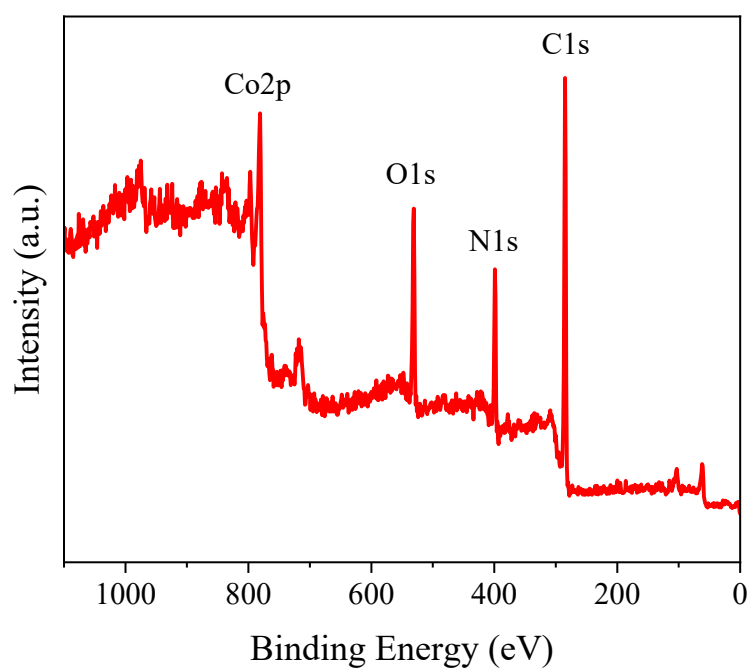


**Fig. S8** Full scan survey XPS spectrum for ZIF-67/CC-24.

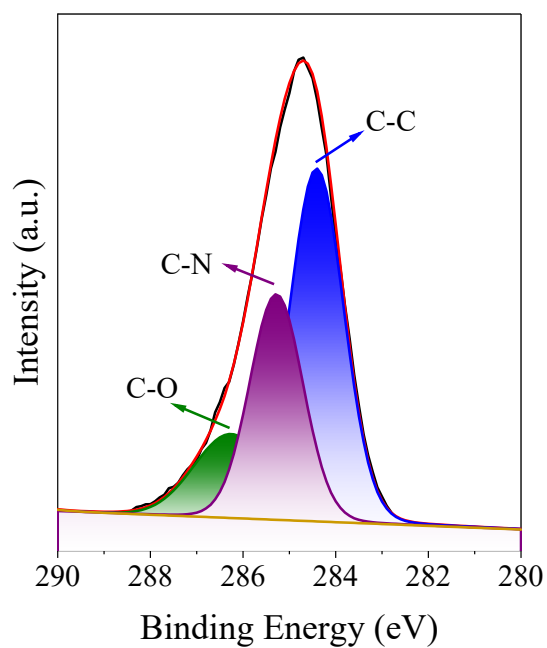


**Fig. S9** High-resolution XPS C1s spectrum of ZIF-67/CC.

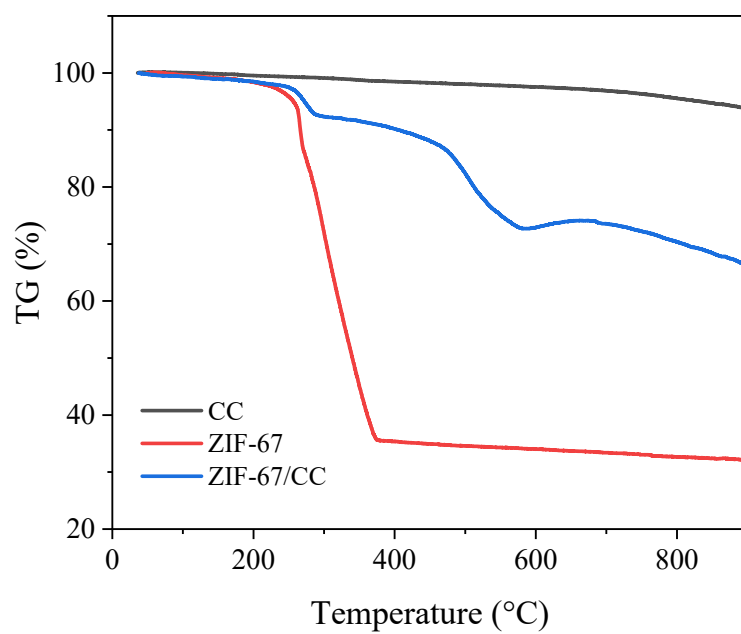


**Fig. S10** TGA curves of ZIF-67/CC, CC and ZIF-67 powders.



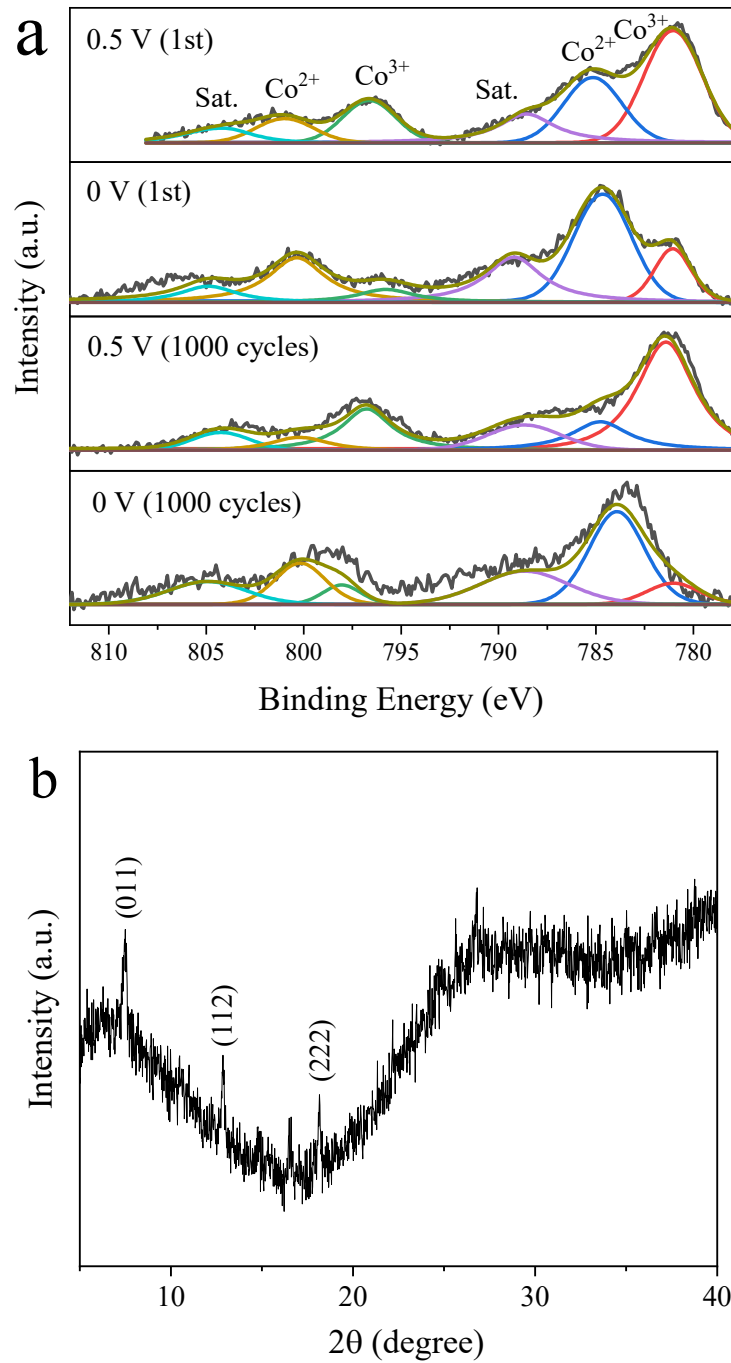


**Fig. S11** (a) XPS spectra of Co 2p and (b) XRD pattern of ZIF-67/CC electrode after cycling.

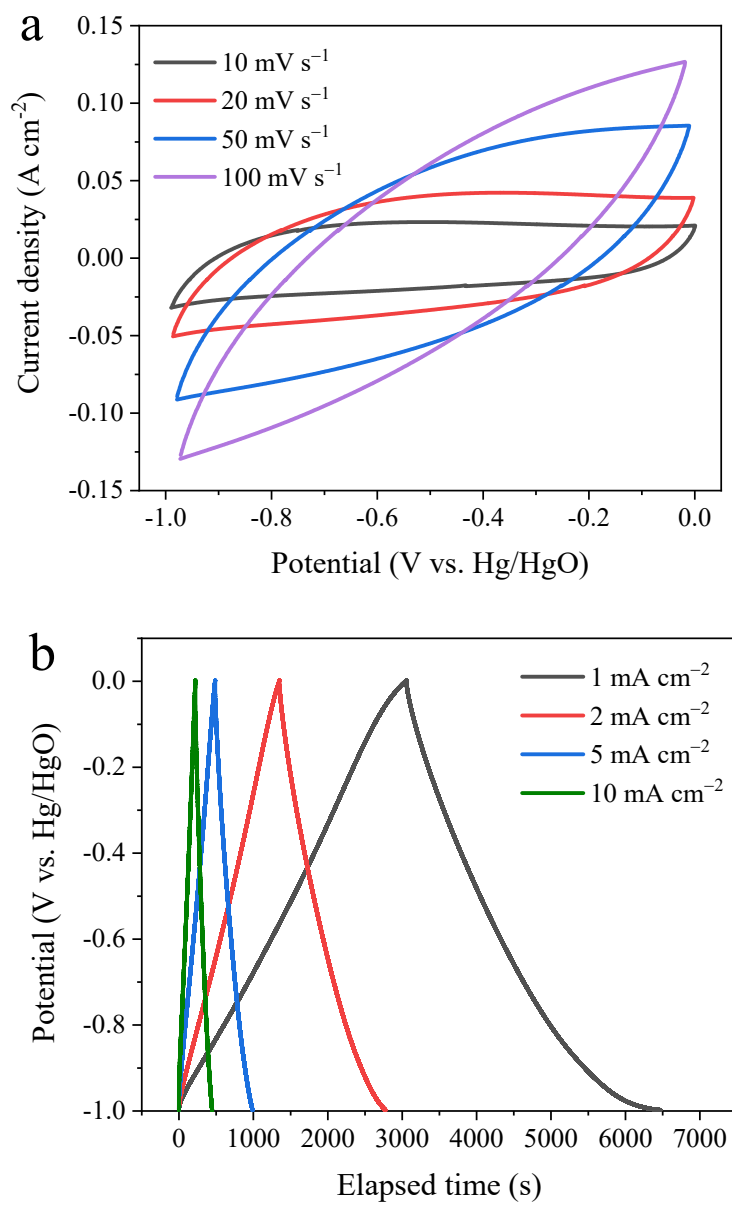


**Fig. S12** (a) CV curves of AC/CC electrode at different scan rates. (b) Galvanostatic charge-discharge curves of AC/CC electrode at different current densities.

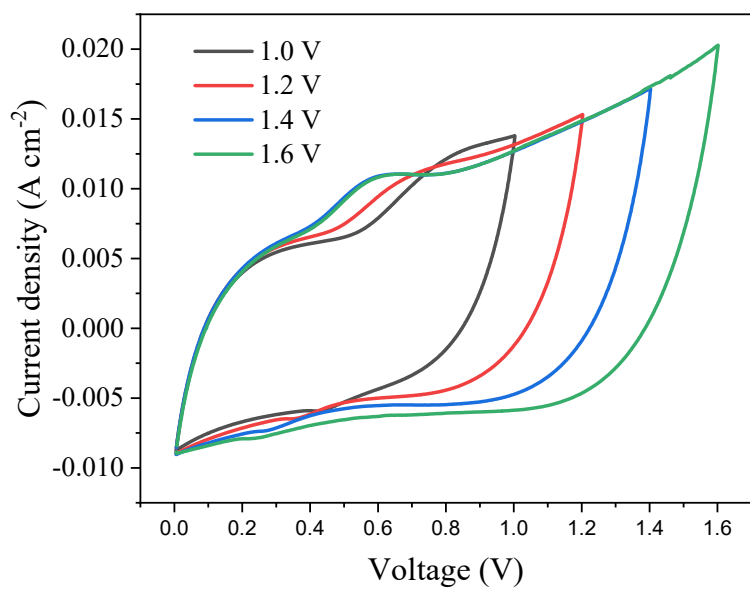


**Fig. S13** CV curves of ZIF-67/CC//AC/CC ASSC device collected within different potential windows at  $10 \text{ mV s}^{-1}$ .

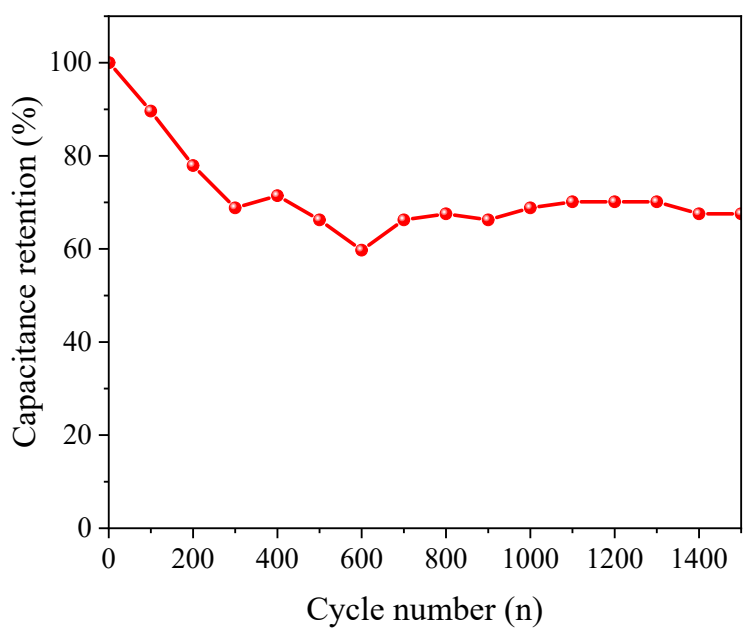


**Fig. S14** Cycling performance of ZIF-67/CC//AC/CC ASSC device at  $10 \text{ mA cm}^{-2}$ .

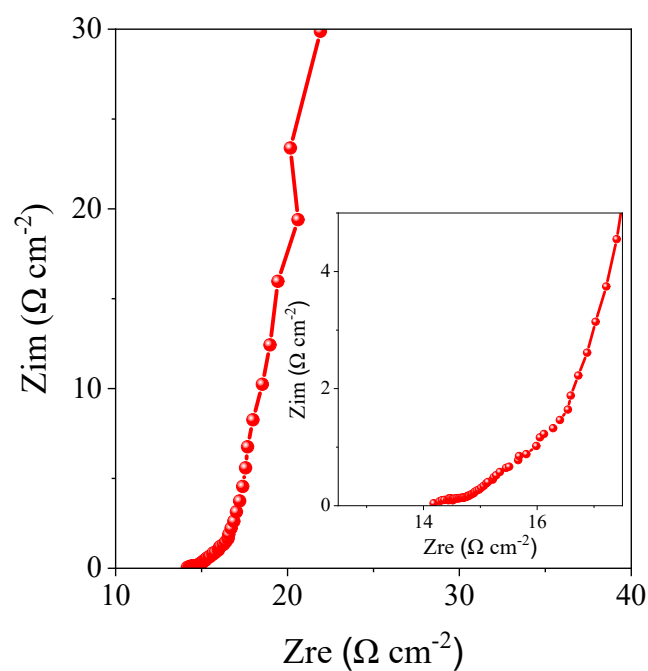


**Fig. S15** Nyquist plot of the ASSC device.

**Table S1** Capacitive performance comparison of reported MOF materials.

Materials	Electrolyte	Current (A g <sup>-1</sup> )	Capacitances (F g <sup>-1</sup> )	Rate capability (%)	Cyclic stability (%/cycles)	Ref.
Cu-CAT NWAs	3 M KCl	0.5	202	66 (0.5-10 A g <sup>-1</sup> )	80/5000	[11]
ZIF-67/PEDOT	1 M H <sub>2</sub> SO <sub>4</sub>	1	107	55 (0.5-10 A g <sup>-1</sup> )	85/2000	[18]
ZIF-67 microflowers	1 M KOH	1	188.7	73 (0.5-8 A g <sup>-1</sup> )	105/3000	[35]
PPy/Ni-CAT-NWs	3 M KCl	0.1	284	70 (0.1-0.6 A g <sup>-1</sup> )	-	[36]
rGO/Cu-MOF fiber	1 M KCl	0.005 (mA cm <sup>-1</sup> )	2.17 (mF cm <sup>-1</sup> )	-	69/1000	[37]
ZIF-67/CC	1M LiOH	1	257	91 (1-10 mA cm <sup>-2</sup> )	99/10000	This work

**Table S2** Comparison of areal energy and power densities for some reported MOF-based devices.

Devices	Mass loading (mg cm <sup>-2</sup> )	Electrolyte	Energy density (mWh cm <sup>-2</sup> )	Power density (mW cm <sup>-2</sup> )	Ref.
Ni@Z67//AC	-	3M KOH	3.8×10 <sup>-2</sup>	0.7	[38]
Ti <sub>3</sub> C <sub>2</sub> T <sub>x</sub> /ZIF-67/CoV <sub>2</sub> O <sub>6</sub> //AC	1-1.5	3M KOH	3.6×10 <sup>-2</sup>	0.75	[26]
ZIF-PPy*	10	PVA/Na <sub>2</sub> SO <sub>4</sub> gel	1.1×10 <sup>-2</sup>	1.44	[39]
PANI-ZIF67-CC*	4	PVA/H <sub>2</sub> SO <sub>4</sub> gel	4.4×10 <sup>-3</sup>	0.48	[4]
Co-MOF/NF//AC	6.656	2M KOH	1.7	4.0	[40]
Co-MOF/graphenen//AC	2.6	6M KOH	2.1×10 <sup>-2</sup>	2.21	[41]
CoNi-MOF//AC	1	1M KOH	2.9×10 <sup>-2</sup>	1.5	[12]
CC/CoNi-MOF//g-CNT	1.48	1M KOH	0.264	0.704	[42]
Ni-CAT/NiCo-LDH/NF//AC	1.5	1M KOH	9.3×10 <sup>-2</sup>	18.3	[9]
Cu <sub>3</sub> (HHTP) <sub>2</sub> //PPy	-	PVA/KCl hydrogel	8.8×10 <sup>-5</sup>	4.5×10 <sup>-3</sup>	[43]
Cu-CAT NWAs*	0.5	PVA/KCl gel	5.2×10 <sup>-3</sup>	10 <sup>-4</sup>	[11]
Cu-CAT-NWAs/PPy	2.01	LiCl-PVA gel	2.2×10 <sup>-2</sup>	0.47	[10]
ZIF-67/CC//AC	12	LiOH/PVA gel	380	1600	This work

\* Symmetric supercapacitor